OXFORD

Human Molecular Genetics, 2016, Vol. 25, No. 11 2283–2294

doi: 10.1093/hmg/ddw096
Advance Access Publication Date: 22 March 2016
Original Article

ORIGINAL ARTICLE

Mutations in *C8ORF37* cause Bardet Biedl syndrome (BBS21)

Elise Heon[1,2,3,*,†], Gunhee Kim[4,†], Sophie Qin[3], Janelle E. Garrison[4], Erika Tavares[3], Ajoy Vincent[1,2], Nina Nuangchamnong[5], C. Anthony Scott[6], Diane C. Slusarski[6] and Val C. Sheffield[4]

[1]Department of Ophthalmology and Vision Sciences, The Hospital for Sick Children, Toronto, M5G 1X8 Canada, [2]Department of Ophthalmology and Vision Sciences, University of Toronto, Toronto, M5G 1X8 Canada, [3]Program of Genetics and Genomic Biology, The Hospital for Sick Children, Toronto, M5G 1X8 Canada, [4]Department of Pediatrics, Division of Medical Genetics, Wynn Institute for Vision Research, Carver College of Medicine, [5]Department of Obstetrics and Gynecology, Carver College of Medicine and [6]Department of Biology, University of Iowa, Iowa City, IA 52242, USA

*To whom correspondence should be addressed at: Department of Ophthalmology and Vision Sciences, The Hospital for Sick Children, University of Toronto, Toronto, Ontario, Canada. Tel: +1 416 813-8606; Email: elise.heon@sickkids.ca

Abstract

Bardet Biedl syndrome (BBS) is a multisystem genetically heterogeneous ciliopathy that most commonly leads to obesity, photoreceptor degeneration, digit anomalies, genito-urinary abnormalities, as well as cognitive impairment with autism, among other features. Sequencing of a DNA sample from a 17-year-old female affected with BBS did not identify any mutation in the known BBS genes. Whole-genome sequencing identified a novel loss-of-function disease-causing homozygous mutation (K102*) in *C8ORF37*, a gene coding for a cilia protein. The proband was overweight (body mass index 29.1) with a slowly progressive rod-cone dystrophy, a mild learning difficulty, high myopia, three limb post-axial polydactyly, horseshoe kidney, abnormally positioned uterus and elevated liver enzymes. Mutations in *C8ORF37* were previously associated with severe autosomal recessive retinal dystrophies (retinitis pigmentosa RP64 and cone-rod dystrophy CORD16) but not BBS. To elucidate the functional role of *C8ORF37* in a vertebrate system, we performed gene knockdown in *Danio rerio* and assessed the cardinal features of BBS and visual function. Knockdown of *c8orf37* resulted in impaired visual behavior and BBS-related phenotypes, specifically, defects in the formation of Kupffer's vesicle and delays in retrograde transport. Specificity of these phenotypes to BBS knockdown was shown with rescue experiments. Over-expression of human missense mutations in zebrafish also resulted in impaired visual behavior and BBS-related phenotypes. This is the first functional validation and association of *C8ORF37* mutations with the BBS phenotype, which identifies BBS21. The zebrafish studies hereby show that *C8ORF37* variants underlie clinically diagnosed BBS-related phenotypes as well as isolated retinal degeneration.

[†]These authors contributed equally to this work.

Received: February 1, 2016. **Revised:** March 7, 2016. **Accepted:** March 17, 2016

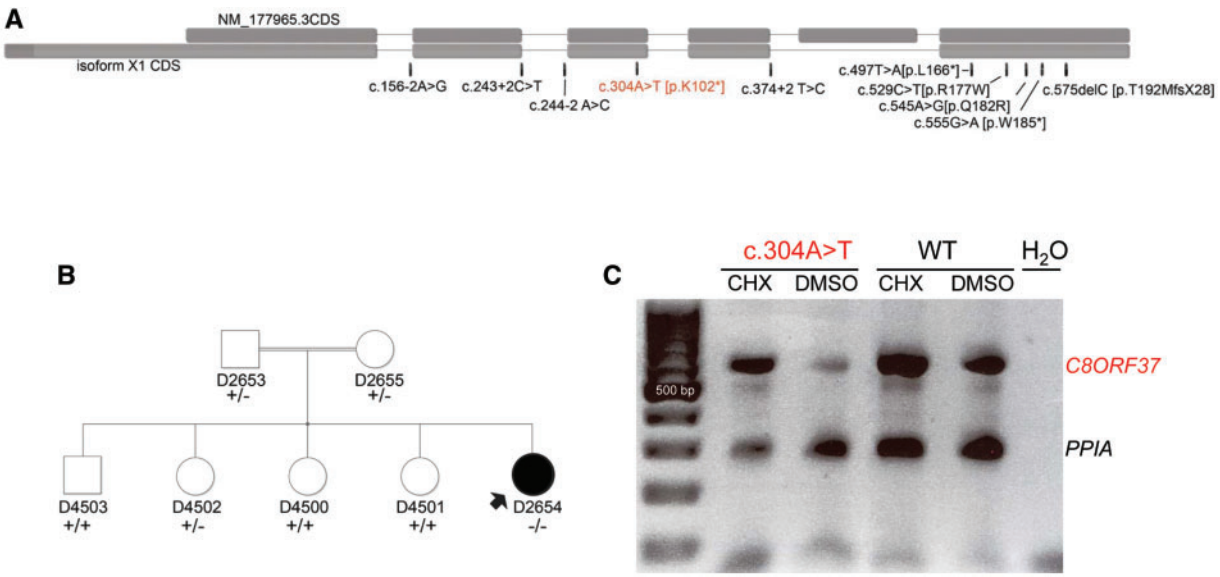

Figure 1. Pedigree, *C8ORF37* genomic structure and NMD assessment. (**A**) Schematic of genomic structure of two *C8ORF37* isoforms with location of the novel mutation (K102*) hereby associated with BBS among the known mutations (associated with severe RP with maculopathy). (**B**) Pedigree showing first-degree consanguinity and family structure. Arrow: proband; −: mutant allele; +: WT allele; clear symbol: not affected; dark symbol: affected. (**C**) Semi-quantitative analysis of RT-PCR to assess the role of NMD. Products are cDNAs derived from lymphoblast cell lines from the patient with the variant c.304A> T and a WT individual for the c.304 position. The effect of treatments with cycloheximide (CHX) and dimethyl sulfoxide (DMSO) show that c.304>T undergoes NMD. Ladder indicates each 100 base pairs, with a strong band corresponding to 500 base pairs. PPIA served as a control.

Introduction

Bardet Biedl syndrome (BBS, MIM209900) is a genetically heterogeneous pleiotropic disorder of autosomal recessive inheritance and is primarily characterized by photoreceptor degeneration, obesity, digit anomalies, genito-urinary anomalies and cognitive impairment (1,2). BBS is considered a ciliopathy, as genes associated with the disease are associated with primary cilia function (3–22). BBS has been an important disease model to highlight the clinical and molecular overlaps that now characterize ciliopathies (23,24). Mutations in BBS genes may also cause other syndromic conditions that mimic BBS or other ciliopathies and result in non-syndromic (isolated) retinal dystrophies such as cone-rod dystrophy (CRD, MIM 120970) and retinitis pigmentosa (RP, MIM 268000) (25,26). The genetic heterogeneity of non-syndromic inherited retinal dystrophies involves over 250 causally associated genetic loci (RETNET, http://www.RETNET.org, last accessed April 19, 2016), a third of which are genes expressed in primary cilia (27).

RP and CRD are inherited photoreceptor degeneration diseases that differ by the predominant photoreceptor cell type involved. The prevalence of RP is 1 in 4000 individuals and 1 in 40 000 individuals for CRD. In both conditions, the vision loss is usually progressive and severe for which there is no treatment at this time. Mutations in *C8ORF37* were recently identified in individuals with autosomal recessive RP type 64 (RP64) and CRD type 16 (CORD16) (27–32). Nine different *C8ORF37* mutations have been reported (Fig. 1A), none of which were associated with BBS (27,32).

The C8ORF37 (NP_808880.1) protein is encoded by six exons (Fig. 1A) and is 207 amino acids in length (NM_177965.3). The overall function and functional domains of C8ORF37 are unknown. *C8ORF37* is expressed ubiquitously in human tissues, with robust expression in the brain, heart and retina (27). C8ORF37 is localized to the base of the photoreceptor connecting cilium (27). As such, it is likely that mutations in this gene disturb intracellular trafficking and can contribute to the pathophysiology of RP, CRD as well as BBS.

In this study, we report that a novel homozygous *C8ORF37* mutation causes BBS. Using gene knockdown in zebrafish, we observed visual impairment and BBS-specific phenotypes, specifically Kupffer's vesicle (KV) formation defects and melanosome transport delay. We also tested the pathogenicity of two previously reported missense mutations associated with retinal dystrophies (32) by using established BBS-related phenotypes in zebrafish and visual function assessment (33). In this study, we took advantage of rapid disease modeling in zebrafish to elucidate the role of the *Danio rerio c8orf37* in BBS-related functions and vision thus providing phenotype–genotype correlation for BBS21.

Results

Clinical assessment

A 12-year-old Caucasian female, born to consanguineous parents (Fig. 1B), was initially referred for progressive myopia (2012) with no significant family or personal history of vision loss or health issues and underwent a thorough assessment.

Ocular phenotype: high myopia with slowly progressive rod-cone degeneration

Correction of the myopia of −9.0 + 2.50 axis 110° (oculus dexter [OD]) and −10.0 + 2.25 axis 80° (oculus sinister [OS]) led to a best-corrected visual acuity of 20/40 in either eye which remained unchanged over 3 years (ages 12–15 years). Retinal atrophy was seen around the optic nerve (peripapillary) and inferiorly, which findings were in keeping with myopic degenerative changes (Fig. 2A). However, mild vessel attenuation and a flat looking retina were observed and suggestive of RP (Fig. 2A). Fundus autofluorescence showed a paramacular ring of hyper-AF; increased AF was also noted at the fovea, whereas inferior retina revealed a

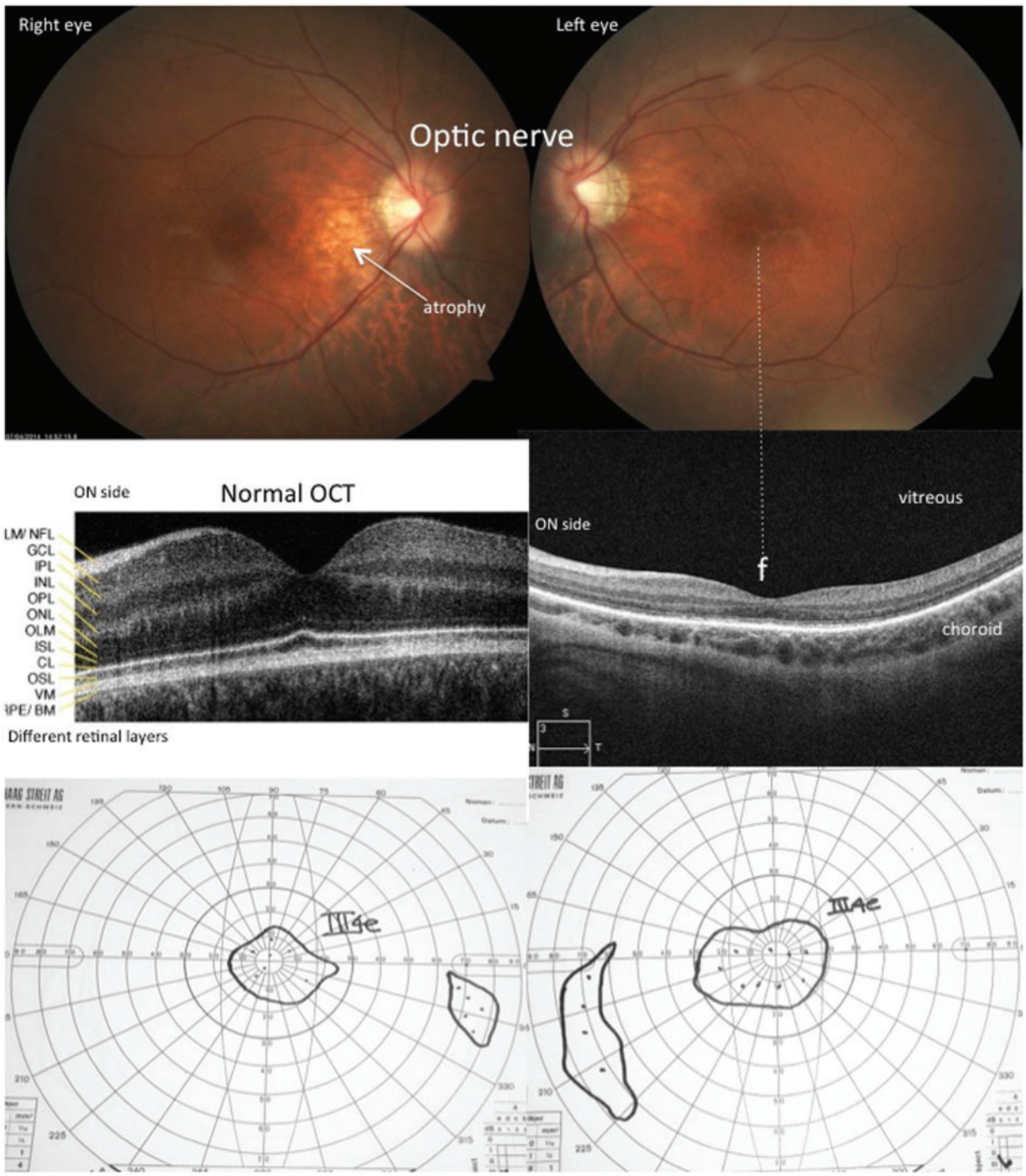

Figure 2 Clinical phenotype at age 16 years. Upper panel: photograph of the retina of both eyes at the age of 16 years centered on the optic nerve (ON) and macula, the center of which is the fovea (f, dotted line). The paler area around the ON represents retinal atrophy and the foveal reflex is blunt. Middle panel: this is correlated by the OCT of left eye centered of the foveal. The foveal depression is reduced compared to the normal OCT, which corresponds to the blunt reflex on the photograph. The foveal depression is also thicker with the continuation of the GCL and IPL layers, which is diagnostic of a mild hypoplasia of the fovea. The resolution of the OCT allows the differentiation of the retinal layers, defined on the normal OCT; ILM/NFL: inner limiting membrane/nerve fiber layer; GCL: ganglion cell layer; IPL: inner plexiform layer; INL: inner nuclear layer; OPL: outer plexiform layer; INL: inner nuclear layer; OLM: outer limiting membrane; ISL: inner segment layer; CL: ciliary line; OSL: outer segment layer; RPE/BM: retinal pigment epithelium/Bruch's membrane. The photoreceptor layer includes ISL, CL and OSL. D and lower panel: Goldmann visual fields (III4e isopter) show constriction OS (left eye) more than the right eye (OD). The dotted red line traces a normal field diameter of 120° (horizontal) × 100° (vertical).

speckled pattern of AF, suggesting diffuse retinal pigment epithelium dysfunction (Fig. 2B). Spectral-domain optical coherence tomography of the central retina showed areas of disruption of the photoreceptor outer segment (OS) - inner segment (IS) junction the external limiting membrane, a network-like structure that is situated at the bases of the rods and cones, appeared to be reasonably preserved at the macula (Fig. 2C). The central retinal thickness, on the lower end of normal, did not change between

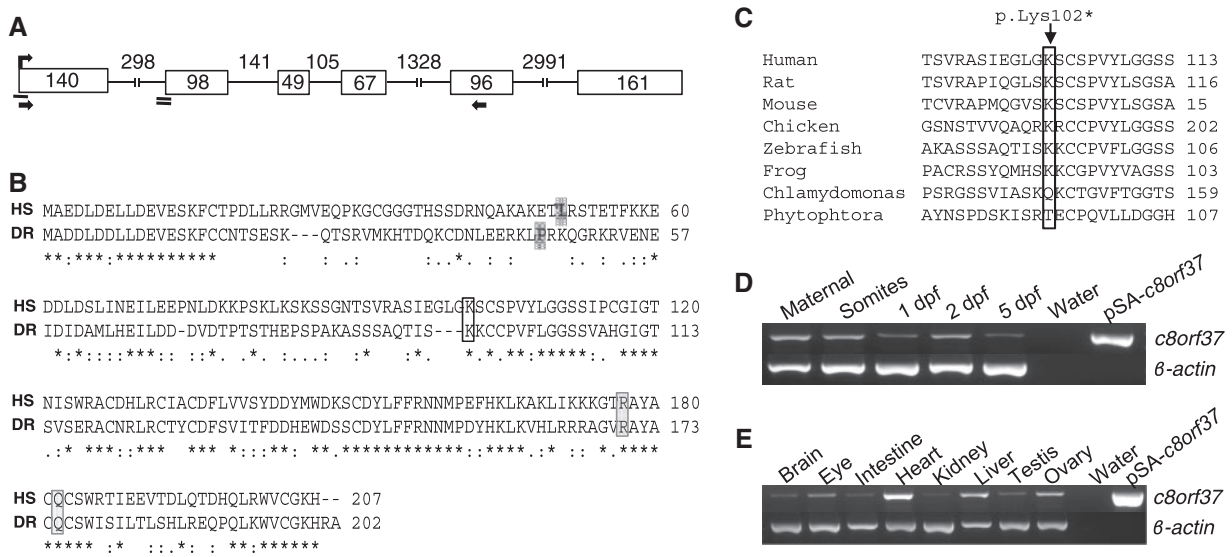

Figure 3 *Danio rerio* as a model to study the functional roles of *c8orf37*. (**A**) Schematic presentation of genomic structure of *c8orf37*. The protein-coding region of *c8orf37* has six exons. Translation start site is depicted with a curved arrow; the sites of ATG and splice MOs are shown with single and double bars below exons 1 and 2, respectively. The primers used for RT-PCR in (**D**) and (**E**) are flanked with black arrows. (**B**) Protein conservation between human (HS) and zebrafish (DR). The alignment was performed via ClustalO using the following protein sequences: *Homo sapiens* (HS) (NP_808880.1) and *D. rerio* (DR) (XP_003200284.2). There is evolutionary conservation of reported mutations in RP64 and CORD16 patients (p.Leu166, p.Arg177, p.Gln182 and p.Trp185) as well as our novel mutation site boxed in black: p.Lys102. Two missense mutation sites studied in this report (p.Arg177 and p.Gln182) are boxed in gray. The first amino acid of exon2 in HS and DR is highlighted in gray. (**C**) Partial alignment of C8ORF37 orthologs. The alignment that was performed with ClustalO shows evolutionary conservation of the novel mutation, p.Lys102, among human, rat (NP_001007747.1), mouse (NP_080281.3), chicken (XP_418346.2), zebrafish and frog (XP_002931575.1). (**D**) Temporal expression profiles of *c8orf37* by RT-PCR. Robust expression of *c8orf37* between 10 and 13 somite stages and 5 dpf enabled us to elucidate BBS-related and visual function phenotypes of *c8orf37*. *β*-actin served as a control. (**E**) Expression of *c8orf37* in adult fish tissues by RT-PCR. The ubiquitous expression of *c8orf37* was robust in the tissues tested. *β*-actin served as a control.

2011 (OD: 202 μm; OS: 196 μm) and 2014 (OD: 199 μm; OS: 200 μm). A grade 1 foveal hypoplasia (34) was coincidentally observed with no retinal re-organization and a well-preserved retinal lamination (Fig. 2C).

The full-field electroretinogram (ERG) recordings were severely decreased suggesting a progressive rod-cone dystrophy and recording was still measurable at 16 years of age. More specifically, the dim light scotopic ERG (rods) was non-detectable. The bright flash ERG (7.6 cds.m-2) showed reduced but detectable a-wave (40 microvolts and 33 microvolts in the RE and LE, respectively); the b-waves were smaller than the a-wave. The cone ERGs were also severely attenuated in both eyes. Although her central visual acuity remained stable over 3 years, the fields of vision constricted by 50%, to less than 20 degrees (Fig. 2D and E), meeting the criteria of legal blindness. Color vision was not measurable using the HRR (Hardy Rand Ritler test) plates by the age of 14 years and her contrast vision was reduced.

Systemic findings meet the diagnostic criteria of BBS

The patient was overweight (with a body mass index of 29.1 at 15 years) and had three limbs post-axial polydactyly, a horseshoe kidney (with normal function), mild learning difficulty and elevated liver enzymes (alanine transaminase: 81 units/l). Liver ultrasound was normal but she had an abnormally positioned uterus. Hearing, behavior and brain magnetic resonance imaging were normal.

Molecular assessment

Patient genotyping identified a novel homozygous K102 mutation in C8ORF37*

Mutational analysis of known BBS disease-causing genes using a Clinical Laboratory Improvement Amendments-approved laboratory first showed a heterozygous variant in BBS4 (K46R) that was predicted to be benign, and no deletion was identified using microarray analysis. Whole-genome sequencing covered 97% of the whole-genome sequence and 98.8% of the known exons. The genome-wide SNP-heterozygous/homozygous ratio (Ti/Tv) was less than would be expected for a proband of a non-consanguineous family (~2), at 1.527 (35). From the whole-genome filtering (Supplementary Material, Fig. S1), 24 variants were selected according to our criteria of conservation and pathogenicity prediction (Supplementary Material, Table S1). The only variant involving a gene associated with retinal degeneration (27,31) was a novel homozygous nonsense variant (NM_177965.3: c.304A > T/p.K102*) in *C8ORF37*, which was highly conserved (Fig. 3C) and segregated with disease status in the family (Fig. 1B). The mutation was within a large homozygous region (32 Mb) on chromosome 8 (Supplementary Material, Fig. S2) and was not reported in any control databases (1000 genomes, NHLBI, cg and dbSNP). Only one heterozygous K102* allele was observed in ExAc from 121 116 individuals (frequency 8.257×10^{-6}). K102* was predicted to be disease causing by Mutation Taster with probability of 0.999 and deleterious according to Combined Annotation Dependent Depletion (CADD)_Phred. In addition, c.304A > T met the criteria of pathogenicity as defined by the American College of Medical Genetics and Genomics standards and guidelines (36).

K102 leads to nonsense-mediated decay*

Nonsense-mediated decay (NMD), a process by which cells recognize and degrade mRNA containing premature stop mutations to prevent toxic effects of truncated peptides, was activated by the nonsense mutation c.304A > T (Fig. 1C). The *C8ORF37* reverse transcriptase-polymerase chain reaction

(RT-PCR) product from the cDNA matched with the control transcript with higher expression for the gene, NM_177965.3. The RT-PCR showed a difference in transcript level between the mutant samples treated with cycloheximide, a translation inhibitor, versus the samples treated with dimethyl sulfoxide (DMSO). In comparison, there were no differences in transcript levels with either treatment in the wild-type (WT) samples.

Mutations in C8ORF37 are a rare cause of BBS

Direct sequencing of the *C8ORF37* coding sequence was performed in 53 unrelated clinically diagnosed BBS patients without mutations in known BBS genes based on molecular testing. No additional disease-causing mutations were identified in *C8ORF37*.

c8orf37 is expressed during zebrafish embryonic development and in adult tissues

The *D. rerio* chromosome 16 open reading frame of human C8ORF37 (c16h8orf37) protein (XP_003200284.2) is encoded by six exons and is 202 amino acids in length (XM_003200236.3) (Fig. 3A and B). The predicted zebrafish ortholog shows 44% amino acid identity (61% homology) to human C8ORF37 (Clustal2.1) (Fig. 3B). Four of the *C8ORF37* mutations sites in exon 6 (L166, R177, Q182 and W185) reported to cause retinal degeneration (27) and the site of the novel nonsense mutation (K102*) are conserved in zebrafish (Fig. 3B and C) as well as in rat, mouse, chicken and frog (Fig. 3C). The implication of mutating R177 and Q182 were hereby specifically explored. *c8orf37* is ubiquitously expressed during early zebrafish development and in adult tissues including the eye, brain, heart and kidney (Fig. 3D and E). The high conservation in the pathogenic amino acid sequences of zebrafish C8orf37 compared with that of human C8ORF37 and the comparable expression of *c8orf37* and *C8ORF37* through embryogenesis to adulthood supports the role of *D. rerio* as a good model system to study the potential pathogenicity of human mutations in this gene.

Knockdown of *c8orf37* in zebrafish results in BBS-related phenotypes

To establish the functional role of *c8orf37* in syndromic as well as non-syndromic retinal degeneration, we performed gene knockdown experiments in the zebrafish model. This approach was previously successful in evaluating hypomorphic mutations associated with RP in genes that also caused different syndromic disorders (37). For gene knockdown, antisense morpholino oligonucleotides (MO) targeting the *c8orf37* translation start target (ATG MO) and the splice junction of intron1 and exon2 (Splice MO) were injected into 1–2 cell stage embryos at different doses. RT-PCR of splice morphants verified that knockdown persisted out through 5 dpf (data not shown). The gross morphology of both the ATG and splice morphants appeared normal without visible defects such as bent body axis and renal cysts. To verify our hypothesis that *C8ORF37* causes BBS, we evaluated the *c8orf37* morphants for BBS-related phenotypes such as defects in KV formation and retrograde melanosome transport, in addition to visual behavior.

KV formation is impaired in c8orf37 morphants

Kuppfer's vesicle (KV) is a ciliated organ that develops from the dorsal forerunner cells and is found transiently in the posterior tailbud of developing zebrafish embryos from 10 to 30 h post-fertilization (hpf). The KV is analogous to the mammalian node and plays a role in left–right axis patterning. During the somite stage, the segmentation period, the ciliated KV normally forms in the tailbud of the zebrafish and can be readily inspected under a microscope. KV morphology was scored between the 10 and 13 somite stages, and reduction of the KV size to less than notochord width or its absence was considered defective (Fig. 4A). Similar to what has been seen in BBS (24,33), knockdown of *c8orf37* using either the ATG MO or splice MO resulted in statistically significant KV defects in a dose-dependent manner. At the highest dose (8 ng splice MO), approximately 53% (57/107) of embryos displayed KV defects, while the lower doses of 5 ng ATG MO or 4 ng Splice MO generated 20% and 29% defects, respectively (Fig. 4C). Analysis of ATG morphants demonstrates a general decrease in vesicle size and cilia content (Fig. 4B).

Delayed retrograde melanosome transport in c8orf37 morphants

Pigment distribution in zebrafish serves as a model for cellular transport and specific motors lead to disperse melanosome (anterograde transport) or the perinuclear aggregation of melanosomes (retrograde transport) in response to environmental or chemical cues. A cardinal feature of knocking down BBS function is a delay in the rate of retrograde intracellular transport within the melanophore (9,25–27). We determine the rate of melanosome transport to the perinuclear regions in *c8orf37* morphants. Day 5 larvae reared in a dark background had melanophores with dispersed melanosomes (Fig. 4D; before). Trafficking of melanosomes from the periphery to the perinuclear region is stimulated by addition of epinephrine (Fig. 4D; after). The time to reach the perinuclear region was measured in individual larva and the average time of retrograde melanosome trafficking for each group was plotted (Fig. 4E). WT and control MO injected larvae responded within 1.60 ± 0.05 min and 1.76 ± 0.01 min, respectively. ATG morphants (2.5 and 5.0 ng) and splice morphants (8 ng) showed statistically significant delays in melanosome transport ($P < 0.05$) (Fig. 4E). These data show that knockdown of *c8orf37* function generates a KV defect and delays in melanosome transport, known cardinal features of zebrafish knockdown of BBS gene expression.

c8orf37 morphants have impaired visual behavior

Because mutations in *C8ORF37* were also associated with severe non-syndromic retinal dystrophies in patients, we tested the visual function of morphants. Zebrafish larvae have an adaptive escape response of change in swimming direction when exposed to sudden changes in light (Supplementary Material, Fig. S3A). We have used this vision startle assay in analysis of several genes associated with human visual disorders (37,38–41). The numbers of larval responses to five visual startle stimuli were recorded. Knockdown of the Cone-Rod Homeobox (*crx*) was used as a control of visually non-responsive morphants. WT embryos and control morphants typically respond >4 times and *crx* morphants average ~2 times (Fig. 5). Both ATG and splice morphants showed a statistically significant decrease in visual startle responses with splice morphants compared to controls demonstrating greater impairment in a MO-dose-dependent manner: 2.5 ng (3.58 ± 0.4, *t*-test $P < 0.05$), 5 ng (3.46 ± 0.32, *t*-test $P < 0.05$) and 8 ng (1.98 ± 0.22, analysis of variance [ANOVA] with Tukey $P < 0.01$). Indeed, the 8-ng splice morphant response showed no significant difference from *crx* morphants (Fig. 5).

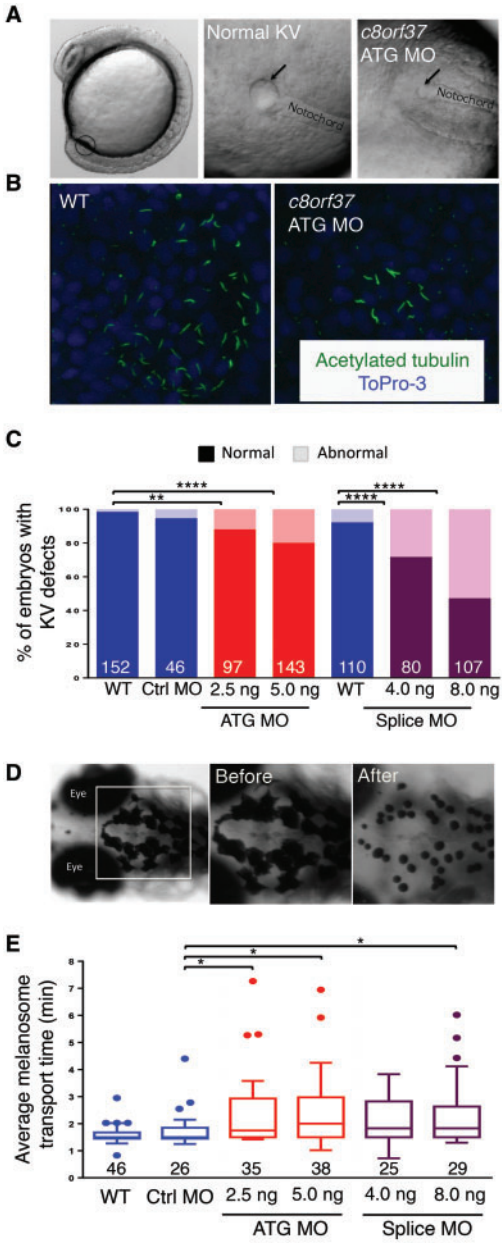

Figure 4 Knockdown of *c8orf37* reveals extraocular BBS-related defects. (**A**) The KV phenotype was assessed at 10–13 somite stages evaluating the size of the vesicle (arrow) relative to the notochord and was abnormal in the ATG morphant. (**B**) Immunohistochemisty of KVs. The confocal images of KVs confirmed abnormal vesicle formation in the ATG morphants and suggested reduced number of motile cilia in it. Acetylated tubulin served as a marker for cilia and toPro-3 stained nuclei. (**C**) Graphic presentation of KV defects analyses. Abnormal KV formation, either reduced or absent, was observed in the both ATG and splice morphants in a MO-dose dependent manner. Data present number and percentage of embryos with KV defects. $^{**}P < 0.01$ and $^{****}P < 0.0001$ with Fisher's exact probability test. Number of larvae tested is in histogram bar. (**D**) Melanosome transport assay at 5 dpf in a control animal. After epinephrine shows the perinuclear distribution. To address the rate of retrograde intracellular trafficking, the time for a dark-adapted larva in epinephrine containing solution to retrieve melanosomes in the head area was measured. The time differences are showed in (**E**). (**E**) Graphic presentation of melanosome transport assay. Delayed melanosome transport was observed in both ATG and splice morphants in a MO-dose-dependent manner. $^{*}P < 0.05$ with one-way ANOVA with Tukey adjustment. The splice morphants injected with 4 ng of MO also delayed trafficking significantly ($P < 0.01$) when compared to WT with Student *t*-test. The numbers of larvae tested are noted below lower whisker.

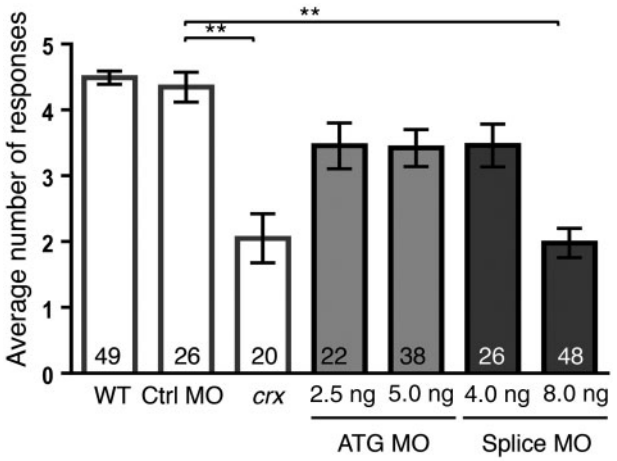

Figure 5 The vision startle responses. Graphic displays of the vision startle assay responses of the ATG and splice MO, both showing impaired visual function. Eight nanograms of Splice MO injection produced the most profound vision defects. Ctrl MO (normal) and *crx* MO (blind) were used as controls. Data present mean ± SEM. $^{**}P < 0.01$ with one-way ANOVA with Tukey multiple comparison procedure. The number of animals studied is indicated in italics in the histogram bar.

Specificity of c8orf37 knockdown and gene product rescue

To validate the specificity of MO knockdown and to functionally validate the non-syndromic retinal dystrophy-associated alleles, we tested the extent to which full-length mRNAs of *c8orf37* rescued *c8orf37* morphant defects. We selected splice MO (8 ng) as it produced robust knockdown phenotypes. We performed sequential injections introducing *c8orf37* RNA (~200 pg) followed by 8 ng Splice MO to directly assess the impact of the RNA compared to MO only and RNA only siblings. Embryos injected with WT *c8orf37* RNA appeared morphologically normal. *c8orf37* RNA injected in the splice morphants rescued MO-induced KV defects (Fig. 6A), melanosome transport delay (Fig. 6B), and the visual defect (Fig. 6C).

Functional analysis of human missense mutations

We have established that knockdown of *c8orf37* generated BBS-like phenotypes and visual impairment and demonstrated that wt-*c8orf37* can rescue knockdown defects. We next evaluated the functional properties of human missense mutations and the relationship of the non-syndromic *c8orf37* mutations with BBS-related phenotypes. Our previous work evaluating the extent to which an allele can suppress the knockdown defects has revealed both syndromic and non-syndromic aspects to BBS3 mutations (38).

To evaluate the level of protein expression in the injected embryos, we placed N-terminal myc-tags on WT and missense *c8orf37* constructs. Zebrafish embryos were injected with RNA of the WT or missense forms. Protein was isolated from RNA injected embryos at day 5 and the abundance of myc-tagged product was determined by western blot. WT, R177W and Q182R *c8orf37* products were expressed (Supplementary Material, Fig. S5). Because of the activation of NMD by K102* shown in Human, this allele was not characterized. We next determined if myc-tagged wt-*c8orf37* suppressed the MO knockdown, similar to untagged form. Sequential injection of RNAs and *c8orf37* splice MO demonstrated that both the untagged and myc-tagged form suppress the MO-induced KV defect. *c8orf37* morphants showed 31% KV defects, while the untagged and tagged

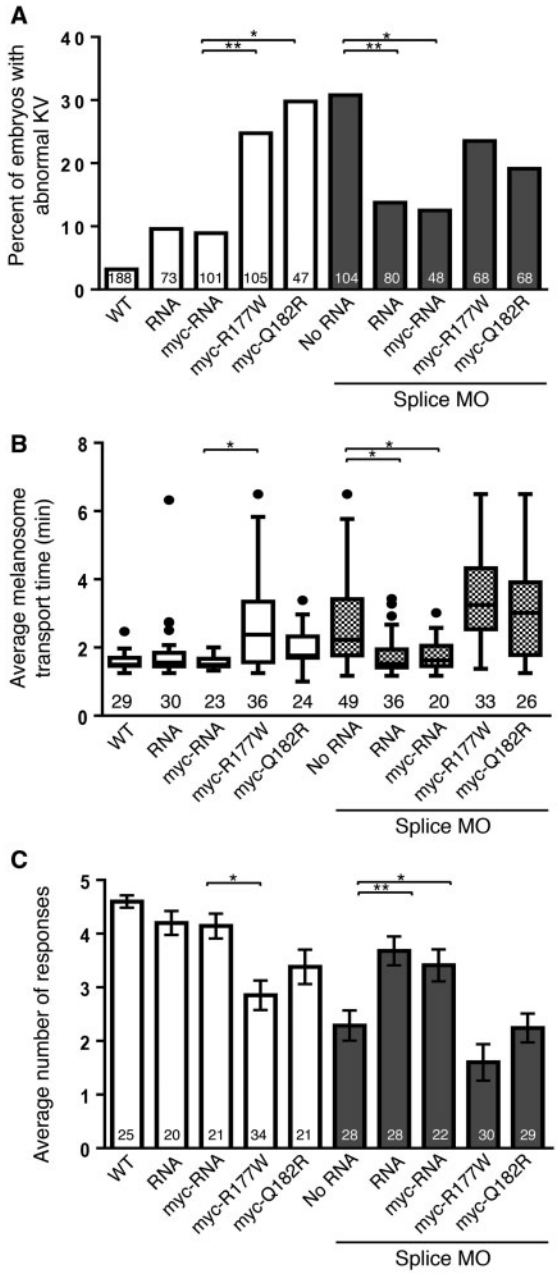

Figure 6 Evaluation of missense mutations. (**A**) Graphic presentation of KV defects analyses. Both nascent form of synthetic RNA and myc-RNA produced normal KV formation in the splice morphants. Both the R177W and the Q182R mutant showed a KV defect. Mutant RNAs did not rescue the KV defects in the morphants but overexpression of either form induced significant KV malformation. Data present number and percentage of embryos with an abnormal KV. *$P < 0.05$ and **$P < 0.01$ with Fisher's exact probability test. (**B**) Graphic presentation of melanosome transport assay. Delayed melanosome transport was normalized in the RNA or myc-RNA co-injected morphants. The data show that the R177W mutation itself induces a retrograde transport defect by delaying melanosome transport time. *$P < 0.05$ with one-way ANOVA with Tukey adjustment. The number of larvae tested is shown in each histogram bar. (**C**) Graphic presentation of the vision startle assays. Both RNA and myc-RNA were able to rescue the vision impairment in the splice morphants, while overexpression of the mutant form of RNAs failed to reverse the knockdown-driven vision impairments. In fact, the expression of the mutant RNAs alone resulted in significant vision defects. Data present mean ± SEM. *$P < 0.05$ and **$P < 0.01$ with one-way ANOVA with Tukey adjustment. The numbers of embryos studied are shown in the histogram bar.

RNA plus MO were at 13.8% (Fisher's exact, $P < 0.01$) and 12.5% (Fisher's exact, $P < 0.05$), respectively (Fig. 6A).

Melanosome transport rates were evaluated at 5 dpf in the sequentially injected embryos. Both tagged and untagged forms rescued the MO defect (Fig. 6B). The melanosome transport rate in splice morphants (2.65 ± 0.17 min) was reduced to 1.76 ± 0.09 min ($P < 0.05$) in untagged and 1.80 ± 0.11 min ($P < 0.05$), in the myc-tagged RNA plus MO groups. Finally, both tagged and untagged WT *c8orf37* rescued the MO-induced vision defect with morphants responding 2.29 ± 0.28 times, and untagged and tagged RNA plus MO responding 3.68 ± 0.27 times and 3.41 ± 0.30 times, respectively (Fig. 6C). We showed that the N-terminal myc tag did not interfere with C8orf37 protein function.

The pathogenicity of two of the reported *C8ORF37* missense mutations associated with retinal degeneration was determined using overexpression of the mutant RNAs (R177W-RNA and Q182R-RNA) in WT zebrafish. Overall, embryos injected individually with R177W-RNA or Q182R-RNA showed normal morphology. However, expression of R177W and Q182R generated somewhat different phenotypes relative to KV formation, melanosome transport and vision. Injection of R177W-RNA into WT embryos induced statistically significant KV formation defects (Fig. 6A), melanosome transport delays (Fig. 6B) and visual impairment (Fig. 6C), while Q182R-RNA injected embryos displayed statistically significant KV formation defects (Fig. 6A). Overexpression of Q182R did not disrupt melanosome transport (Fig. 6B). Statistically significant visual impairment was observed when data were analyzed with one-tailed Student's *t*-test ($P = 0.03$) (Fig. 6C). These data support the pathogenicity of both mutations.

We next evaluated the extent to which R177W and Q182R expression rescued knockdown phenotypes with sequential injection of Splice MO and RNA. Sequential injection of R177W-RNA with the Splice MO failed to rescue the KV defect (23.5% of embryos with abnormal KV formation compared to 31% in Splice MO only) (Fig. 6A) and melanosome transport delay (Fig. 6B). While R177W-RNA plus Splice MO appeared to have decreased visual response rates compared to Splice MO only, it was not statistically significant. In summary, for all phenotypes examined (KV defects, melanosome transport and vision), sequential injection of Splice MO with either R177W or Q182R RNA failed to significantly rescue the phenotype compared to Splice MO only. Relative to the KV defect, Q182R-RNA alone was not significantly different than Splice MO-alone, and although Q182R-RNA in morphants showed a 19% KV defect (compared to 30% MO), it was not significantly different than Splice MO only (Fig. 6A). Q182R-RNA alone did not significantly alter melanosome transport nor did it suppress Splice MO-induced melanosome transport delay (Fig. 6B). Moreover, Q182R-RNA in morphants showed the same visual defect as MO-alone (Fig. 6C). The failure of either mutation to rescue knockdown with MO supports the pathogenicity of R177W and Q182R.

Discussion

The novel *C8ORF37* p.K102* variant reported here is the first association of BBS with *C8ORF37* (*BBS21*). C8ORF37 is not predicted to be a component of the BBSome nor based on homology would it be expected to be a component of the BBS gene network. However, our zebrafish model system showed that *in vivo c8orf37* knockdown led to the zebrafish "BBS phenotypes," which supports that the homozygous p.K102* variant found in a single BBS patient is likely the cause of the signs observed. Specifically, we determined that MO knockdown of *c8orf37* results in delayed retrograde melanosome transport,

abnormalities in KV morphogenesis, in addition to an abnormal visual function. In addition, we validated the pathogenicity of *C8ORF37* mutations and showed that the K102*-containing transcript undergoes NMD. These findings support an interaction of *C8ORF37* with the BBS gene network, yet to be characterized.

C8ORF37 (MIM614500) is a ciliary cytoplasmic protein that has no significant sequence homology to any other human protein. It has been given its own protein class: the retinal maintenance protein superfamily and has no known function. *C8ORF37* is ubiquitously expressed (http://www.gtexportal.org/home/gene/C8orf37, last accessed April 19, 2016) and co-localizes with polyglutamylated tubulin at the base of the primary cilium in human retinal pigment epithelium cells and at the base of the photoreceptor connecting cilium (27). It is proposed to have interactions with NRF1 (alpha palindromic-binding protein), which function links the transcriptional modulation of key metabolic genes to cellular growth and development. The ubiquitous expression patterns throughout development are typical of BBS genes and further support *C8ORF37* being involved with primary cilia function and implicated in the development of BBS [(http://bgee.unil.ch/bgee/bgee, last accessed April 19, 2016), (http://www.ncbi.nlm.nih.gov/unigene, last accessed April 19, 2016), (http://www.proteinatlas.org/, last accessed April 19, 2016) and (http://www.ebi.ac.uk, last accessed April 19, 2016)]. While *C8ORF37* has not been previously reported to be involved in BBS, two siblings with retinal disease associated with a *C8ORF37* mutation (*C8ORF37* c.156-2A->G) also had polydactyly on the right foot or hand (7,8). Whether this finding was truly isolated is unclear as signs of BBS may be mild and overlooked if not functionally significant (42).

In humans, allelic heterogeneity of *C8ORF37* leads to different retinal degeneration phenotypes (27–32) and now includes that of BBS (BBS21). As study of other ciliary proteins has shown, mutations can lead to important phenotype heterogeneity (42,43). The effect of an early null mutation (p.K102*) may explain the full blown BBS phenotype. The potential modifying role of the likely benign heterozygous *BBS4* (p.K46R) on *C8ORF37* p.K102* expression is yet to be determined. The recent report of a known *C8ORF37* mutation (R177W) associated with a BBS-like phenotype (44) also suggests that early disruption of *C8ORF37* may lead to a more syndromic phenotype with extra-ocular features. Our work supports that *C8ORF37* mutations associate with syndromic and non-syndromic retinal degeneration.

Zebrafish have been a useful model in allowing validation of a range of conserved novel variants. In this study, we find that WT *c8orf37* can rescue knockdown defects related to BBS and to vision, unlike the missense mutations p.Q182R and p.R177W that do not globally suppress the knockdown phenotypes. Based on the zebrafish work, it could be that missense mutations result in a less deleterious effect than an early null mutation, as indicated by the human data.

Although *C8ORF37* mutations are a rare cause of BBS (BBS21), such an association is important and suggests that patients with *C8ORF37* mutations should have a medical workup to assess the potential presence of BBS features including obesity, renal abnormalities, diabetes and hypertension. Furthermore, this expands the components of the BBS-related network. How C8ORF37 interacts with the BBS protein network including the BBSome remains to be determined.

Materials and Methods

This work was approved by the Hospital for Sick Children (Toronto, Canada) Ethics Review Board respecting the Tenets of the Declaration of Helsinki and the University Animal Care and Use Committee at the University of Iowa (IA). All oligonucleotides used are listed in Supplementary Material, Table S1.

Clinical assessment details

The patient was recruited through the Ocular Genetics Clinic of the Hospital for Sick Children (Toronto) and met the clinical diagnostic criteria of BBS (1,45). Phenotype information collected included a comprehensive eye exam and kinetic visual fields (Goldmann perimeter). The spectral-domain optical coherence tomography (Cirrus, Carl Zeiss Meditec) was also used to provide high-resolution (axial resolution: 5 μm) cross-sectional images of the central retinal layers. Central retinal thickness referred to the 1 mm diameter circle centered on the fovea (46). The recording of the full-field ERG met the International Society for Clinical Electrophysiology of Vision standards (47).

Molecular assessment of the patient

Genotyping of patient

Genotyping on blood derived DNA first excluded the known BBS genes using a Clinical Laboratory Improvement Amendments-approved laboratory. We followed this testing with standard whole-genome re-sequencing using mated gapped reads was performed by Complete Genomics (http://www.completegenomics.com/, last accessed April 19, 2016) (48). Mapping to genome assembly GRCh37/hg19 and annotation was done in our in-house facility; TCAG (http://www.tcag.ca/facilities/dnaSequencingSynthesis.html, last accessed April 19, 2016). Details of the filtering steps are available in Supplementary Material, Fig. S1. Potential disease-causing variants were validated according to internal protocols (Supplementary Material, Fig. S1). Novel mutations were assessed using information from the literature and various mutations databases. The potential effect of novel variants was predicted using publicly available software: Polyphen-2 (49) and SIFT (50) followed by segregation analysis and determination of allele frequency in the normal population.

Testing of *NMD* on lymphoblast cell lines

To determine whether the variant c.304A > T (p.K102*) causes NMD (51–54), total RNA was extracted from the lymphoblast cell lines (patient and control) with RNeasy (Qiagen, Hilden, Germany) according to manufacturer's instructions. Subsamples of the cells (106) were treated with 1.5 mg of cyclohexamide (stock 100 mg/ml in DMSO, 4 hours incubation at 37°C), which inhibits translation (NMD) (55) and an equivalent subsample with only DMSO (15 μl). RT-PCR used primers flanking *C8ORF37* exon 3 (*C8ORF37*-mRNA, Supplementary Material, Table S1) where the nonsense variant is located and co-amplified with those of the Cyclophilin A (PPIA, Supplementary Material, Table S1) a housekeeping gene to control for experimental variation. The *C8ORF37* cDNA RT-PCR products from mutant and control were validated by Sanger sequencing.

c8orf37 Zebrafish Model

Zebrafish were maintained in compliance with the University Animal Care and Use Committee at the University of Iowa. Embryos were collected from natural spawning and staged as described previously (56,57).

RT-PCR

Total RNA was extracted from pools of WT embryos using the Total RNA Mini Kit (Tissue) (IBI Scientific® Peosta, IA) at the following stages: maternal (2–4 cells), 10–13 somites stage, 1 day post-fertilization (dpf), 2 dpf and 5 dpf as well as from the adult brain, eye, intestine, heart, kidney, liver, testis and ovary (oocytes). cDNA was synthesized utilizing oligo DT primers, the expression of *c8orf37* was evaluated using primers spanning exon1 and exon5 (*c8orf37*-f and -r, Supplementary Material, Table S1) and β-actin expression served as a control (Supplementary Material, Table S1).

Knockdown with antisense oligonucleotide morpholinos (MO)

In this article, the predicted zebrafish ortholog of human *C8ORF37 is* referred to as *c8orf37*. We used two different antisense MO to knock down *c8orf37*: antisense *c8orf37* MOs targeting the translation start site (ATG MO, Supplementary Material, Table S1) or intron1-exon2 junction (Splice MO, Supplementary Material, Table S1) were purchased from Gene Tools (LLC, Philomath, OR). As the phenotype associated with previously reported mutations, we validated the pathogenicity of two previous reported variants. We characterized the phenotype of two missense mutations of *C8ORF37* reported in patients with nonsyndromic retinal degeneration: p.R177W and p.Q182R. We assessed the effects of the different MOs on visual behavior, KV formation and retrograde intracellular trafficking *in vivo* (melanosome transport assay), which are phenotypes known to be associated with BBS. MOs were air-pressure-injected into one- to two-cell staged embryos at concentrations ranging from 2 to 10 ng. The efficacy of splice MO on transcript was assayed by RT-PCR using cDNA generated from pools of MO-injected embryos (morphants) at 10–13 somite and 5 dpf stages using primers *c8orf37*-rt-f and *c8orf37*-rt-r (Supplementary Material, Table S1). Cone-rod homeobox (crx) MO injection served as a control for the vision startle assay (58,59) and standard control MO injection served as an injection control (Supplementary Material, Table S1).

Zebrafish BBS-related phenotypes assessment

Core BBS phenotypes in zebrafish have been previously established and encompass reduced cilia in the KV, reduced KV size and delayed cellular transport (9,25–27).

Morphological analysis and immunohistochemistry of KV

The KV is a transient ciliated organ formed in the tailbud of somite-stage zebrafish (60–62). Morphological analysis of KVs in live 10–13 stage embryos (~14 hpf) was performed using a stereoscope and size was scored relative to the width of the notochord (33,63). Representative live embryos were photographed with a Zeiss Axiocam camera. To assess KV, 10–13 somite stage embryos were fixed, stained against acetylated tubulin (Sigma-Aldrich (T7451)), goat anti mouse Alexa Fluor® 488 (Invotrogen (A-21121)) and photographed with an Olympus Confocal microscope (Fluoview FV10i, Olympus Corporation, Tokyo, Japan).

Retrograde melanosome transport assay

BBS knockdown was shown to delay the rate of melanosome retrograde transport (33,40,63). To disperse the melanosomes, 5-day-old larvae were incubated overnight in the dark and then treated with epinephrine (final concentration 500 μg/ml, Sigma E4375). The time for melanosomes to move to the perinuclear area was documented under a microscope (Olympus SZX7, objective lens 2X).

Vision startle response assay

A behavioral assay based on a startle response by a light evoked stimulus was performed as previously described (38,40,63–65). In short, 5-day-old larvae were light adapted for at least 1 h in advance and then evoked by 1 s block in bright light intensity for five times spaced 30 s apart. Swimming patterns were observed under a microscope. At the end of the assay, larvae were probed with a blunt needle. Those that failed to respond to mechanical stimuli were excluded from the data analysis.

Analysis of retinal morphology

After the vision startle response assay, larvae were fixed with 4% paraformaldehyde in phosphate-buffered saline, infiltrated with 15% sucrose, 30% sucrose followed by 100% optimal cutting temperature compound (OCT, Sakura, Tokyo, Japan). Larvae were cryo-sectioned at 10–12 μm thicknesses and stained according to a standard H&E staining protocol. Images were taken with an Olympus IX71 inverted microscope. The length of the individual photoreceptors was measured using Image J program. Coronal sections of the photoreceptors of the central retina of the brain side from three of WT and six *c8orf37* morphants were studied.

Cloning zebrafish c8orf37 and generation of two human missense mutations

Full-length *c8orf37* was amplified using cDNA synthesized from 5 dpf embryos with the primers (*c8orf37-EcoRI*-f and *XhoI-r*, Supplementary Material, Table S1), cloned utilizing the StrataClone Blunt PCR Cloning Kit (Agilent Technologies, Santa Clara, CA) and subsequently subcloned into pCS2+. The cloned product was mutagenized using primers *c8orf37* R177W f and r, Q182R f and r in Supplementary Material, Tables S1 and PfuUltraII fusion HS DNA polymerase. PCR products were digested with *EcoRI* and *XhoI* and then subcloned into a pCS2 + MT tagging myc N-terminally. The sequence of all products was verified. The cloned product was mutagenized using primers *c8orf37* R177W f and r, Q182R f and r (Supplementary Material, Table S1) and PfuUltraII fusion HS DNA polymerase. PCR products were digested with *EcoRI* and *XhoI* and then subcloned into a pCS2 + MT tagging myc N-terminally. Bold letters were mutated C->**T**, T->**G** and A->**G** in order. Products were sequenced using SP6 and T7 primers (Supplementary Material, Table S1).

RNA synthesis for rescue studies

Full-length *c8orf37* RNA, N-terminally myc tagged RNA (myc-RNA), myc-R177W RNA and myc-Q182R RNA were *in vitro* transcribed utilizing the mMessagemMachine transcription kit (SP6) (Ambion. Austin, TX). For rescue experiments, synthesized RNA products (100 ng/μl RNAs) were injected into one-cell stage embryos followed by the injection of the splice MO.

Supplementary Material

Supplementary Material is available at *HMG* online.

Acknowledgements

We thank Autumn Marsden and Charles. C. Searby (University of Iowa, IA) for technical support, and Daniele Merico and

Christian Marshall from The Centre of Applied Genomics (The Sick Children Hospital, Toronto, Canada) for WGS filtering pipeline. We also thank Hélène Dollfus, MD, and Corinne Stoetzel who sequenced 44 families to look for C8ORF37 variants (from the Laboratoire de Génétique Médicale INSERM U1112 and Centre de référence pour les affections rares en génétique ophtalmologique (CARGO) (Strasbourg, FRANCE).

Conflict of Interest statement. None declared.

Funding

The Mira Godard Research Fund (to E.H.); The McLaughlin Foundation Accelerator grant (to E.H.); the Ophthalmology Research Fund (to E.H.); US National Institutes of Health grants (R01EY011298 and R01EY017168 to V.C.S.); Carver Charitable Trust (V.C.S.); Howard Hughes Medical Institution (V.C.S.) and Cardiovascular Interdisciplinary Research Fellowship (Institutional NRSA HL007121 to J.E.G.).

References

1. Beales, P.L., Warner, A.M., Hitman, G.A., Thakker, R. and Flinter, F.A. (1997) Bardet-Biedl syndrome: a molecular and phenotypic study of 18 families. *J. Med. Genet.*, **34**, 92–98.
2. Kerr, E.N., Bhan, A. and Héon, E. (2016) Exploration of the cognitive, adaptive and behavioral functioning of patients affected with Bardet-Biedl syndrome. *Clin. Genet.*, **89**, 426–433.
3. Kwitek-Black, A.E., Carmi, R., Duyk, G.M., Buetow, K.H., Elbedour, K., Parvari, R., Yandava, C.N., Stone, E.M. and Sheffield, V.C. (1993) Linkage of Bardet-Biedl syndrome to chromosome 16q and evidence for non-allelic genetic heterogeneity. *Nat. Genet.*, **3**, 392–396.
4. Leppert, M., Baird, L., Anderson, K.L., Otterud, B., Lupski, J.R. and Lewis, R.A. (1994) Bardet-Biedl syndrome is linked to DNA markers on chromosome 11q and is genetically heterogeneous. *Nat. Genet.*, **7**, 108–112.
5. Sheffield, V.C., Carmi, R., Kwitek-Black, A., Rokhlina, T., Nishimura, D., Duyk, G.M., Elbedour, K., Sunden, S.L. and Stone, E.M. (1994) Identification of a Bardet-Biedl syndrome locus on chromosome 3 and evaluation of an efficient approach to homozygosity mapping. *Hum. Mol. Genet.*, **3**, 1331–1335.
6. Carmi, R., Rokhlina, T., Kwitek-Black, A.E., Elbedour, K., Nishimura, D., Stone, E.M. and Sheffield, V.C. (1995) Use of a DNA pooling strategy to identify a human obesity syndrome locus on chromosome 15. *Hum. Mol. Genet.*, **4**, 9–13.
7. Young, T.L., Penney, L., Woods, M.O., Parfrey, P.S., Green, J.S., Hefferton, D. and Davidson, W.S. (1999) A fifth locus for Bardet-Biedl syndrome maps to chromosome 2q31. *Am. J. Hum. Genet.*, **64**, 900–904.
8. Katsanis, N., Beales, P.L., Woods, M.O., Lewis, R.A., Green, J.S., Parfrey, P.S., Ansley, S.J., Davidson, W.S. and Lupski, J.R. (2000) Mutations in MKKS cause obesity, retinal dystrophy and renal malformations associated with Bardet-Biedl syndrome. *Nat. Genet.*, **26**, 67–70.
9. Ansley, S.J., Badano, J.L., Blacque, O.E., Hill, J., Hoskins, B.E., Leitch, C.C., Kim, J.C., Ross, A.J., Eichers, E.R., Teslovich, T.M. et al. (2003) Basal body dysfunction is a likely cause of pleiotropic Bardet-Biedl syndrome. *Nature*, **425**, 628–633.
10. Badano, J.L., Ansley, S.J., Leitch, C.C., Lewis, R.A., Lupski, J.R. and Katsanis, N. (2003) Identification of a novel Bardet-Biedl syndrome protein, BBS7, that shares structural features with BBS1 and BBS2. *Am. J. Hum. Genet.*, **72**, 650–658.
11. Nishimura, D.Y., Swiderski, R.E., Searby, C.C., Berg, E.M., Ferguson, A.L., Hennekam, R., Merin, S., Weleber, R.G., Biesecker, L.G., Stone, E.M. et al. (2005) Comparative genomics and gene expression analysis identifies BBS9, a new Bardet-Biedl syndrome gene. *Am. J. Hum. Genet.*, **77**, 1021–1033.
12. Chiang, A.P., Beck, J.S., Yen, H.J., Tayeh, M.K., Scheetz, T.E., Swiderski, R.E., Nishimura, D.Y., Braun, T.A., Kim, K.Y., Huang, J. et al. (2006) Homozygosity mapping with SNP arrays identifies TRIM32, an E3 ubiquitin ligase, as a Bardet-Biedl syndrome gene (BBS11). *Proc. Natl. Acad. Sci. U S A.*, **103**, 6287–6292.
13. Stoetzel, C., Laurier, V., Davis, E.E., Muller, J., Rix, S., Badano, J.L., Leitch, C.C., Salem, N., Chouery, E., Corbani, S. et al. (2006) BBS10 encodes a vertebrate-specific chaperonin-like protein and is a major BBS locus. *Nat. Genet.*, **38**, 521–524.
14. Stoetzel, C., Muller, J., Laurier, V., Davis, E.E., Zaghloul, N.A., Vicaire, S., Jacquelin, C., Plewniak, F., Leitch, C.C., Sarda, P. et al. (2007) Identification of a novel BBS gene (BBS12) highlights the major role of a vertebrate-specific branch of chaperonin-related proteins in Bardet-Biedl syndrome. *Am. J. Hum. Genet.*, **80**, 1–11.
15. Leitch, C.C., Zaghloul, N.A., Davis, E.E., Stoetzel, C., Diaz-Font, A., Rix, S., Alfadhel, M., Lewis, R.A., Eyaid, W., Banin, E. et al. (2008) Hypomorphic mutations in syndromic encephalocele genes are associated with Bardet-Biedl syndrome. *Nat. Genet.*, **40**, 443–448.
16. Tammachote, R., Hommerding, C.J., Sinders, R.M., Miller, C.A., Czarnecki, P.G., Leightner, A.C., Salisbury, J.L., Ward, C.J., Torres, V.E., Gattone, V.H. 2nd et al. (2009) Ciliary and centrosomal defects associated with mutation and depletion of the Meckel syndrome genes MKS1 and MKS3. *Hum. Mol. Genet.*, **18**, 3311–3323.
17. Kim, S.K., Shindo, A., Park, T.J., Oh, E.C., Ghosh, S., Gray, R.S., Lewis, R.A., Johnson, C.A., Attie-Bittach, T., Katsanis, N. and Wallingford, J.B. (2010) Planar cell polarity acts through septins to control collective cell movement and ciliogenesis. *Science*, **329**, 1337–1340.
18. Otto, E.A., Hurd, T.W., Airik, R., Chaki, M., Zhou, W., Stoetzel, C., Patil, S.B., Levy, S., Ghosh, A.K., Murga-Zamalloa, C.A. et al. (2010) Candidate exome capture identifies mutation of SDCCAG8 as the cause of a retinal-renal ciliopathy. *Nat. Genet.*, **42**, 840–850.
19. Marion, V., Stutzmann, F., Gerard, M., De Melo, C., Schaefer, E., Claussmann, A., Helle, S., Delague, V., Souied, E., Barrey, C. et al. (2012) Exome sequencing identifies mutations in LZTFL1, a BBSome and smoothened trafficking regulator, in a family with Bardet–Biedl syndrome with situs inversus and insertional polydactyly. *J. Med. Genet.*, **49**, 317–321.
20. Aldahmesh, M.A., Li, Y., Alhashem, A., Anazi, S., Alkuraya, H., Hashem, M., Awaji, A.A., Sogaty, S., Alkharashi, A., Alzahrani, S. et al. (2014) IFT27, encoding a small GTPase component of IFT particles, is mutated in a consanguineous family with Bardet-Biedl syndrome. *Hum. Mol. Genet.*, **23**, 3307–3315.
21. Scheidecker, S., Etard, C., Pierce, N.W., Geoffroy, V., Schaefer, E., Muller, J., Chennen, K., Flori, E., Pelletier, V., Poch, O. et al. (2014) Exome sequencing of Bardet-Biedl syndrome patient identifies a null mutation in the BBSome subunit BBIP1 (BBS18). *J. Med. Genet.*, **51**, 132–136.
22. Bujakowska, K.M., Zhang, Q., Siemiatkowska, A.M., Liu, Q., Place, E., Falk, M.J., Consugar, M., Lancelot, M.E., Antonio, A., Lonjou, C. et al. (2015) Mutations in IFT172 cause isolated

retinal degeneration and Bardet-Biedl syndrome. *Hum. Mol. Genet.*, **24**, 230–242.
23. Zaghloul, N.A. and Katsanis, N. (2009) Mechanistic insights into Bardet-Biedl syndrome, a model ciliopathy. *J. Clin. Invest.*, **119**, 428–437.
24. Mykytyn, K. and Sheffield, V.C. (2004) Establishing a connection between cilia and Bardet-Biedl Syndrome. *Trends Mol. Med.*, **10**, 106–109.
25. Mockel, A., Perdomo, Y., Stutzmann, F., Letsch, J., Marion, V. and Dollfus, H. (2011) Retinal dystrophy in Bardet-Biedl syndrome and related syndromic ciliopathies. *Prog. Retin. Eye Res.*, **30**, 258–274.
26. Schaefer, E., Zaloszyc, A., Lauer, J., Durand, M., Stutzmann, F., Perdomo-Trujillo, Y., Redin, C., Bennouna Greene, V., Toutain, A., Perrin, L. et al. (2011) Mutations in SDCCAG8/NPHP10 Cause Bardet-Biedl Syndrome and are associated with penetrant renal disease and absent polydactyly. *Mol. Syndromol.*, **1**, 273–281.
27. Estrada-Cuzcano, A., Neveling, K., Kohl, S., Banin, E., Rotenstreich, Y., Sharon, D., Falik-Zaccai, T.C., Hipp, S., Roepman, R., Wissinger, B. et al. (2012) Mutations in C8orf37, encoding a ciliary protein, are associated with autosomal-recessive retinal dystrophies with early macular involvement. *Am. J. Hum. Genet.*, **90**, 102–109.
28. Jinda, W., Taylor, T.D., Suzuki, Y., Thongnoppakhun, W., Limwongse, C., Lertrit, P., Suriyaphol, P., Trinavarat, A. and Atchaneeyasakul, L.O. (2014) Whole exome sequencing in Thai patients with retinitis pigmentosa reveals novel mutations in six genes. *Invest. Ophthalmol. Vis. Sci.*, **55**, 2259–2268.
29. Katagiri, S., Hayashi, T., Yoshitake, K., Akahori, M., Ikeo, K., Gekka, T., Tsuneoka, H. and Iwata, T. (2015) Novel C8orf37 mutations in patients with early-onset retinal dystrophy, macular atrophy, cataracts, and high myopia. *Ophthalmic Genet.*, **37**, 68–75.
30. Lazar, C.H., Mutsuddi, M., Kimchi, A., Zelinger, L., Mizrahi-Meissonnier, L., Marks-Ohana, D., Boleda, A., Ratnapriya, R., Sharon, D., Swaroop, A. et al. (2015) Whole exome sequencing reveals GUCY2D as a major gene associated with cone and cone-rod dystrophy in Israel. *Invest. Ophthalmol. Vis. Sci.*, **56**, 420–430.
31. Ravesh, Z., El Asrag, M.E., Weisschuh, N., McKibbin, M., Reuter, P., Watson, C.M., Baumann, B., Poulter, J.A., Sajid, S., Panagiotou, E.S. et al. (2015) Novel C8orf37 mutations cause retinitis pigmentosa in consanguineous families of Pakistani origin. *Mol. Vis.*, **21**, 236–243.
32. van Huet, R.A., Estrada-Cuzcano, A., Banin, E., Rotenstreich, Y., Hipp, S., Kohl, S., Hoyng, C.B., den Hollander, A.I., Collin, R.W. and Klevering, B.J. (2013) Clinical characteristics of rod and cone photoreceptor dystrophies in patients with mutations in the C8orf37 gene. *Invest. Ophthalmol. Vis. Sci.*, **54**, 4683–4690.
33. Yen, H.J., Tayeh, M.K., Mullins, R.F., Stone, E.M., Sheffield, V.C. and Slusarski, D.C. (2006) Bardet-Biedl syndrome genes are important in retrograde intracellular trafficking and Kupffer's vesicle cilia function. *Hum. Mol. Genet.*, **15**, 667–677.
34. Thomas, M.G., Kumar, A., Mohammad, S., Proudlock, F.A., Engle, E.C., Andrews, C., Chan, W.M., Thomas, S. and Gottlob, I. (2011) Structural grading of foveal hypoplasia using spectral-domain optical coherence tomography a predictor of visual acuity? *Ophthalmology*, **118**, 1653–1660.
35. Zhang, Y., Li, B., Li, C., Cai, Q., Zheng, W. and Long, J. (2014) Improved variant calling accuracy by merging replicates in whole-exome sequencing studies. *Biomed. Res. Int.*, **2014**, 319534.
36. Richards, S., Aziz, N., Bale, S., Bick, D., Das, S., Gastier-Foster, J., Grody, W.W., Hegde, M., Lyon, E., Spector, E. et al. (2015) Standards and guidelines for the interpretation of sequence variants: a joint consensus recommendation of the American College of Medical Genetics and Genomics and the Association for Molecular Pathology. *Genet. Med.*, **17**, 405–424.
37. DeLuca, A.P., Whitmore, S.S., Barnes, J., Sharma, T.P., Westfall, T.A., Scott, C.A., Weed, M.C., Wiley, J.S., Wiley, L.A., Johnston, R.M. et al. (2016) Hypomorphic mutations in TRNT1 cause retinitis pigmentosa with erythrocytic microcytosis. *Hum. Mol. Genet.*, **25**, 44–56.
38. Pretorius, P.R., Baye, L.M., Nishimura, D.Y., Searby, C.C., Bugge, K., Yang, B., Mullins, R.F., Stone, E.M., Sheffield, V.C. and Slusarski, D.C. (2010) Identification and functional analysis of the vision-specific BBS3 (ARL6) long isoform. *PLoS Genet.*, **6**, e1000884.
39. Seo, S., Baye, L.M., Schulz, N.P., Beck, J.S., Zhang, Q., Slusarski, D.C. and Sheffield, V.C. (2010) BBS6, BBS10, and BBS12 form a complex with CCT/TRiC family chaperonins and mediate BBSome assembly. *Proc. Natl. Acad. Sci. U S A.*, **107**, 1488–1493.
40. Pretorius, P.R., Aldahmesh, M.A., Alkuraya, F.S., Sheffield, V.C. and Slusarski, D.C. (2011) Functional analysis of BBS3 A89V that results in non-syndromic retinal degeneration. *Hum. Mol. Genet.*, **20**, 1625–1632.
41. Mei, X., Westfall, T.A., Zhang, Q., Sheffield, V.C., Bassuk, A.G. and Slusarski, D.C. (2014) Functional characterization of Prickle2 and BBS7 identify overlapping phenotypes yet distinct mechanisms. *Dev. Biol.*, **392**, 245–255.
42. Riazuddin, S.A., Iqbal, M., Wang, Y., Masuda, T., Chen, Y., Bowne, S., Sullivan, L.S., Waseem, N.H., Bhattacharya, S., Daiger, S.P. et al. (2010) A splice-site mutation in a retina-specific exon of BBS8 causes nonsyndromic retinitis pigmentosa. *Am. J. Hum. Genet.*, **86**, 805–812.
43. den Hollander, A.I., Roepman, R., Koenekoop, R.K. and Cremers, F.P. (2008) Leber congenital amaurosis: genes, proteins and disease mechanisms. *Prog. Retin. Eye Res.*, **27**, 391–419.
44. Khan, A.O., Decker, E., Bachmann, N., Bolz, H.J. and Bergmann, C. (2016) C8orf37 is mutated in Bardet-Biedl syndrome and constitutes a locus allelic to non-syndromic retinal dystrophies. *Ophthalmic Genet.*, 1–4.
45. Deveault, C., Billingsley, G., Duncan, J.L., Bin, J., Theal, R., Vincent, A., Fieggen, K.J., Gerth, C., Noordeh, N., Traboulsi, E.I. et al. (2011) BBS genotype-phenotype assessment of a multiethnic patient cohort calls for a revision of the disease definition. *Hum. Mutat.*, **32**, 610–619.
46. Early Treatment Diabetic Retinopathy Study Research Group (1991) Classification of diabetic retinopathy from fluorescein angiograms. ETDRS report number 11. *Ophthalmology*, **98**, 807–822.
47. Marmor, M.F., Fulton, A.B., Holder, G.E., Miyake, Y., Brigell, M. and Bach, M. (2009) ISCEV Standard for full-field clinical electroretinography (2008 update). *Doc. Ophthalmol.*, **118**, 69–77.
48. Carnevali, P., Baccash, J., Halpern, A.L., Nazarenko, I., Nilsen, G.B., Pant, K.P., Ebert, J.C., Brownley, A., Morenzoni, M., Karpinchyk, V. et al. (2012) Computational techniques for human genome resequencing using mated gapped reads. *J. Comput. Biol.*, **19**, 279–292.
49. Adzhubei, I.A., Schmidt, S., Peshkin, L., Ramensky, V.E., Gerasimova, A., Bork, P., Kondrashov, A.S. and Sunyaev, S.R. (2010) A method and server for predicting damaging missense mutations. *Nat. Methods*, **7**, 248–249.

50. Kumar, P., Henikoff, S. and Ng, P.C. (2009) Predicting the effects of coding non-synonymous variants on protein function using the SIFT algorithm. *Nat. Protoc.*, **4**, 1073–1081.
51. Barker, G.F. and Beemon, K. (1991) Nonsense codons within the *Rous sarcoma virus* gag gene decrease the stability of unspliced viral RNA. *Mol. Cell. Biol.*, **11**, 2760–2768.
52. Belgrader, P. and Maquat, L.E. (1994) Nonsense but not missense mutations can decrease the abundance of nuclear mRNA for the mouse major urinary protein, while both types of mutations can facilitate exon skipping. *Mol. Cell. Biol.*, **14**, 6326–6336.
53. Rajavel, K.S. and Neufeld, E.F. (2001) Nonsense-mediated decay of human HEXA mRNA. *Mol. Cell. Biol.*, **21**, 5512–5519.
54. Byers, P.H. (2002) Killing the messenger: new insights into nonsense-mediated mRNA decay. *J. Clin. Invest.*, **109**, 3–6.
55. Lareau, L.F., Inada, M., Green, R.E., Wengrod, J.C. and Brenner, S.E. (2007) Unproductive splicing of SR genes associated with highly conserved and ultraconserved DNA elements. *Nature*, **446**, 926–929.
56. Kimmel, C.B., Ballard, W.W., Kimmel, S.R., Ullmann, B. and Schilling, T.F. (1995) Stages of embryonic development of the zebrafish. *Dev. Dyn.*, **203**, 253–310.
57. Westerfield, M. (1993) *The Zebrafish Book: A Guide for the Laboratory Use of Zebrafish (Brachydanio rerio)*. University of Oregon Press, Eugene, OR.
58. Liu, Y., Shen, Y., Rest, J.S., Raymond, P.A. and Zack, D.J. (2001) Isolation and characterization of a zebrafish homologue of the cone rod homeobox gene. *Invest. Ophthalmol. Vis. Sci.*, **42**, 481–487.
59. Shen, Y.C. and Raymond, P.A. (2004) Zebrafish *cone-rod (crx) homeobox* gene promotes retinogenesis. *Dev. Biol.*, **269**, 237–251.
60. Essner, J.J., Amack, J.D., Nyholm, M.K., Harris, E.B. and Yost, H.J. (2005) Kupffer's vesicle is a ciliated organ of asymmetry in the zebrafish embryo that initiates left-right development of the brain, heart and gut. *Development*, **132**, 1247–1260.
61. Hirokawa, N., Tanaka, Y., Okada, Y. and Takeda, S. (2006) Nodal flow and the generation of left-right asymmetry. *Cell*, **125**, 33–45.
62. Kramer-Zucker, A.G., Olale, F., Haycraft, C.J., Yoder, B.K., Schier, A.F. and Drummond, I.A. (2005) Cilia-driven fluid flow in the zebrafish pronephros, brain and Kupffer's vesicle is required for normal organogenesis. *Development*, **132**, 1907–1921.
63. Nachury, M.V., Loktev, A.V., Zhang, Q., Westlake, C.J., Peranen, J., Merdes, A., Slusarski, D.C., Scheller, R.H., Bazan, J.F., Sheffield, V.C. et al. (2007) A core complex of BBS proteins cooperates with the GTPase Rab8 to promote ciliary membrane biogenesis. *Cell*, **129**, 1201–1213.
64. Seo, S., Zhang, Q., Bugge, K., Breslow, D.K., Searby, C.C., Nachury, M.V. and Sheffield, V.C. (2011) A novel protein LZTFL1 regulates ciliary trafficking of the BBSome and Smoothened. *PLoS Genet.*, **7**, e1002358.
65. Easter, S.S., Jr and Nicola, G.N. (1996) The development of vision in the zebrafish (*Danio rerio*). *Dev. Biol.*, **180**, 646–663.